Numerical simulations of long-range plasmons

Aloyse Degiron and David R. Smith

Department of Electrical and Computer Engineering, Duke University, Durham, North Carolina, 27708, USA.

drsmith@ee.duke.edu

Abstract: We present simulations of plasmonic transmission lines consisting of planar metal strips embedded in isotropic dielectric media, with a particular emphasis on the long-range surface plasmon polariton (SPP) modes that can be supported in such structures. Our computational method is based on analyzing the eigenfrequencies corresponding to the wave equation subject to a mixture of periodic, electric and magnetic boundary conditions. We demonstrate the accuracy of our approach through comparisons with previously reported simulations based on the semi-analytical method-of-lines. We apply our method to study a variety of aspects of long-range SPPs, including tradeoffs between mode confinement and propagation distance, the modeling of bent waveguides and the effect of disorder and periodicity on the long-ranging modes.

OCIS codes: (240.6680) Surface Plasmons; (130.2790) Guided waves; (130.3120) Integrated optic devices

References and links

1. J.-C. Weeber, A. Dereux, C. Girard, J. R. Krenn, and J.-P. Goudonnet, "Plasmon polaritons of metallic nanowires for controlling submicron propagation of light," Phys. Rev. B **60,** 9061–9068 (1999).
2. J.-C. Weeber, J. R. Krenn, A. Dereux, B. Lamprecht, Y. Lacroute, and J.-P. Goudonnet, "Near-field observation of surface plasmon polariton propagation on thin metal stripes," Phys. Rev. B **64** 045411 (2001).
3. B. Lamprecht, J.R. Krenn, G. Schider, H. Ditlbacher, M. Salerno, N. Felidj, A. Leitner, and F.R. Aussenegg, "Surface plasmon propagation in microscale metal stripes," Appl. Phys. Lett. **79,** 51–53 (2001).
4. J.-C. Weeber, M.U. González, A.-L. Baudrion, and A. Dereux, "Surface plasmon routing along right angle bent metal strips" Appl. Phys. Lett. **87,** 221101, (2005).
5. P. Berini, "Plasmon-polariton waves guided by thin lossy metal films of finite width: bound modes of symmetric structures," Phys. Rev. B **61,** 10484–10503 (2000).
6. P. Berini, "Plasmon-polariton waves guided by thin lossy metal films of finite width: bound modes of asymmetric structures," Phys. Rev. B **63,** 125417 (2001).
7. R. Charbonneau, P. Berini, E. Berolo, and E. Lisicka-Shrzek, "Experimental observation of plasmon-polariton waves supported by a thin metal film of finite width," Opt. Lett. **52,** 844–846 (2000).
8. R. Charbonneau, N. Lahoud, G. Mattiussi, and P. Berini, "Demonstration of integrated optics elements based on long-ranging surface plasmon polaritons," Opt. Express **13,** 977–984 (2005), http://www.opticsinfobase.org/abstract.cfm?URI=oe-13-3-977.
9. S. Jette-Charbonneau, R. Charbonneau, N. Lahoud, G. Mattiussi, and P. Berini, "Demonstration of Bragg gratings based on long-ranging surface plasmon polariton waveguides," Opt. Express **13,** 4674–4682 (2005), http://www.opticsinfobase.org/abstract.cfm?URI=oe-13-12-4674.
10. P. Berini, R. Charbonneau, N. Lahoud, and G. Mattiussi, "Characterization of long-range surface-plasmon-polariton waveguides" J. Appl. Phys. **98,** 043109 (2005).
11. T. Nikolajsen, K. Leosson, I. Salakhutdinov, and S. I. Bozhevolnyi, "Polymer-based surface-plasmon-polariton stripe waveguides at telecommunication wavelengths," Appl. Phys. Lett. **82,** 668–670 (2003).
12. T. Nikolajsen, K. Leosson, and S. I. Bozhevolnyi, "Surface plasmon polariton based modulators and switches operating at telecom wavelengths," Appl. Phys. Lett. **85,** 5833–5835 (2004).

#9991 - $15.00 USD Received 16 December 2005; revised 31 January 2006; accepted 1 February 2006

13. A. Boltasseva, T. Nikolajsen, K. Leosson, K. Kjaer, M.S. Larsen, and S.I. Bozhevolnyi, "Integrated optical components utilizing long-range surface plasmon polaritons," J. Lightwave Technol. **23,** 413–422 (2005).
14. A. Boltasseva, S.I. Bozhevolnyi, T. Søndergaard, T. Nikolajsen, and K. Leosson, "Compact Z-add-drop wavelength filters for long-range surface plasmon polaritons" Opt. Express **13,** 4237–4243 (2005), http://www.opticsinfobase.org/abstract.cfm?URI=oe-13-11-4237.
15. S.J. Al-Bader, "Optical Transmission on Metallic Wires – Fundamental Modes," IEEE J. Quantum Electron. **40,** 325–329 (2004).
16. Rashid Zia, Anu Chandran, and Mark L. Brongersma, "Dielectric waveguide model for guided surface polaritons," Opt. Lett. **30,** 1473–1475 (2005).
17. H. Raether, *Surface Plasmons* (Springer-Verlag, Berlin, 1988).
18. W. L. Barnes, A. Dereux, and T. W. Ebbesen, "Surface plasmon subwavelength optics," Nature (London) **424,** 824–830 (2003).
19. D.M. Pozar, *Microwave Engineering* (John Wiley & Sons, 1998).
20. D. Sarid, "Long-range surface-plasma waves on very thin metal films," Phys. Rev. Lett. **47,** 1927–1930 (1981).
21. J.J. Burke, G. I. Stegeman, and T. Tamir, "Surface-polariton-like waves guided by thin, lossy metal films," Phys. Rev. B **33,** 5286–5201 (1986).
22. J.P. Kottmann, O.J.F. Martin, D.R. Smith, and S. Schultz, "Spectral response of plasmon resonant nanoparticles with a non-regular shape," Opt. Express **6,** 213–219 (2000), http://www.opticsinfobase.org/abstract.cfm?URI=oe-6-11-213.
23. J.P. Kottmann, O.J.F. Martin, D.R. Smith, and S. Schultz, "Dramatic localized electromagnetic enhancement in plasmon resonant nanowires," Chem. Phys. Lett. **341,** 1–6 (2001).
24. P. B. Johnson and R.W. Christy, "Optical constants of the noble metals," Phys. Rev. B **6,** 4370–4379 (1972).
25. D. Marcuse, "Curvature loss formula for optical fibers," J. Opt. Soc. Am. **66,** 216–220 (1976).
26. J.-P. Berenger, "A perfectly matched layer for the absorption of electromagnetic waves," J. Comput. Phys. **114,** 185–200 (1994).
27. R. Mittra and U. Pekel, "A new look at the perfectly matched layer (PML) concept for the reflectionless absorption of electromagnetic waves," IEEE Microwave Guid. Wave Lett. **5,** 84–86 (1995).
28. J. Takahara, S. Yamagishi, H. Taki, A. Morimoto, and T. Kobayashi, "Guiding of a one-dimensional optical beam with nanometer diameter," Opt. Lett. **22,** 475–477 (1997).
29. G. A. Farias and A. A. Maradudin, " Effect of surface roughness on the attenuation of surface polaritons on metal films," Phys. Rev. B **27,** 7093–7106 (1983).
30. W.L. Barnes, T.W. Preist, S.C. Kitson, and J.R. Sambles, "Physical origin of photonic energy gaps in the propagation of surface plasmons on gratings," Phys. Rev. B **54,** 6227–6244 (1996).
31. W.L. Barnes, S.C. Kitson, T.W. Preist, and J.R. Sambles, "Photonic surfaces for surface-plasmon polaritons," J. Opt. Soc. Am. A **14,** 1654–1661 (1997).
32. P.E. Barclay, K. Srinivasan, M. Borselli, and O. Painter, "Probing the dispersive and spatial properties of photonic crystal waveguides via highly efficient coupling from fiber tapers," Appl. Phys. Lett. **85,** 4–6 (2004).
33. S.A. Maier, M.D. Friedman, P.E. Barclay, and O. Painter, "Experimental demonstration of fiber-accessible metal nanoparticle plasmon waveguides for planar energy guiding and sensing," Appl. Phys. Lett. **86,** 071103 (2005).
34. A. Lai, C. Caloz, and T. Itoh, "Composite right/left-handed transmission line metamaterials," IEEE Microwave Magazine **5,** 34–50 (2004).
35. R. Islam, F. Elek, and G.V. Eleftheriades, "Coupled-line metamaterial coupler having co-directional phase but contra-directiona power flow," Electron Lett. **40,** 315–317 (2004).
36. V.G. Veselago, "The electrodynamics of substances with simultaneously negative values of ε and μ," Sov. Phys. Usp. **10,** 509–514 (1968).
37. D. R. Smith, W. J. Padilla, D. C. Vier, S. C. Nemat-Nasser, and S. Schultz, "Composite medium with simultaneously negative permeability and permittivity," Phys. Rev. Lett. **84,** 4184–4187 (2000).
38. M. Kafesaki, Th. Koschny, R. S. Penciu, T. F. Gundogdu, E. N. Economou, and C. M. Soukoulis "Left-handed metamaterials: detailed numerical studies of the transmission properties," J. Opt. A: Pure Appl. Opt. **7,** S12–S22 (2005).
39. S. O'Brien and J.B. Pendry, "Photonic band-gap effects and magnetic activity in dielectric composites" J. Phys. Condens. Matter **14,** 4035–4044 (2002).
40. K.C. Huang, M.L. Povinelli, and J.D. Joannopoulos, "Negative effective permeability in polaritonic photonic crystals," Appl. Phys. Lett. **85** 543–545 (2004).
41. C. Kittel, *Introduction to Solid State Physics* (Wiley, New York, 1966).

1. Introduction

In response to the needs of miniaturization and increased functionality in optical waveguides, there has been an emergence of wave guiding structures based on the controlled excitation of surface plasmon polaritons (SPPs) [1-16]. SPPs are guided modes at a metal/dielectric inter-

#9991 - $15.00 USD Received 16 December 2005; revised 31 January 2006; accepted 1 February 2006

face that result from the coupling between two-dimensional electromagnetic waves and collective electronic oscillations along the metal surface [17]. SPPs are usually characterized by large electromagnetic fields confined within a subwavelength region near the interface and thus exhibit extreme sensitivity to their immediate environment. Consequently, SPPs are subject to control and modulation by adjustment of the interface parameters, which in turn provides a powerful means to squeeze and manipulate light at a scale smaller than the diffraction limit [18]. These unique properties suggest the pursuit of SPP structures as waveguides in the optical regime that are virtually unconstrained by the wavelengths of the electromagnetic waves they carry. Recently, it has been shown that the excitation of long-range SPP modes along metal strips with subwavelength cross-section [5-16] fulfills this purpose.

Rather than being determined predominantly by the operating wavelength, the SPP mode properties result from the inherent capacitance and inductance per unit length of the planar strip. The SPP strip is thus less a waveguide but more the optical analog of the transmission line common to microwave and radio frequency technology [19], even though only a single conductor is present. A detailed study of the strip SPP transmission line was presented by Berini who modeled straight metal strips with rectangular cross-section by means of the semi-analytical method of lines [5, 6]. Berini showed that the collective SPP modes for the strip geometry can be understood as arising from the coupling between individual SPPs localized near the edges and the corners of the strip. The thickness and width of the strip strongly influence the overlap of the fields and hence the coupling between interface SPP modes; by adjusting the cross-sectional strip geometry, the field localization and rate of attenuation of the mode can be tuned. For example, the attenuation length of certain modes can be dramatically increased by simply decreasing the thickness of the strip, to the point that SPP modes can propagate over distances of centimeters at visible wavelengths–distances orders of magnitude larger than for uncoupled SPPs supported by an isolated metal/dielectric interface [17]. The origin of the increased propagation lengths is that as the metal thickness decreases, the fields of the coupled states become less confined at the strip surface, thus lowering the damping due to absorption in the metal. Among these modes–frequently referred to as *long-range* SPPs [20, 21]–one is of greater practical interest because it has neither a cutoff thickness nor a cutoff frequency and also because its field pattern allows excitation via a simple end-fire technique (e.g., focusing light on the input of the strip). The existence of long-range modes has been confirmed by subsequent simulations [15, 16] and also by experiments on millimeters-long metal strips embedded in isotropic dielectrics [7-14]. Empirical studies have also shown that single symmetric long-range SPP transmission lines can be combined to make passive optical devices (such as junctions or filters) [8, 14] as well as active components such as thermo-optically actuated interferometers and switches [12].

Much of the theoretical analysis on SPP transmission lines has been performed using semi-analytic techniques which, though accurate and powerful, are somewhat restrictive in terms of the geometries that can be solved. The collection of data and simulations on SPP transmission lines accumulated thus far has revealed the extraordinary sensitivity of the modes to the composition and symmetry of the surrounding host materials. This sensitivity is similar to that found in the simulation of plasmonic nanoparticles of arbitrary shape [22, 23]. Although this sensitivity adds considerable complexity to the analysis and design of plasmonic structures, it is also the property that makes such structures so interesting. As the development of useful SPP transmission lines progresses, it is thus useful to apply numerical methods capable of incorporating accurately the exact details of the local geometry, including such factors as the surface roughness of the metal, interface irregularities, periodicity and bending. By incorporating these details, better optimization and increased functionality of SPP transmission lines can be facilitated.

#9991 - $15.00 USD Received 16 December 2005; revised 31 January 2006; accepted 1 February 2006

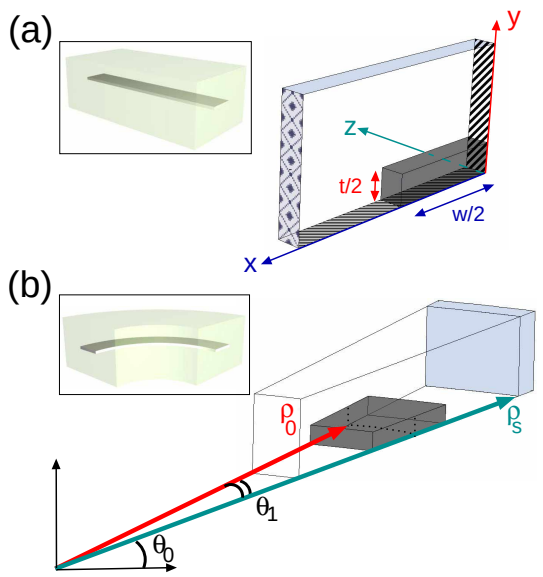

Fig. 1. Unit cell for simulating: (a) a straight waveguide of thickness t and width w – the patterned zones represent the perfect walls placed at the boundaries of the computational domain; (b) a bent waveguide with a mean radius of curvature ρ_0. The colored volume behind the boundary $\rho = \rho_s$ represents a PML. Inserts: 3D views of the two types of structures.

In this paper we apply an eigensolver approach that is capable of solving for the modes of SPP transmission lines of complex geometry and arbitrary material composition. We illustrate the numerical method in Section 2 using the eigensolver module in HFSS (Ansoft), a commercially available finite-element code. The eigensolver in HFSS is particularly useful for this approach because it provides complex eigenfrequencies, enabling the calculation of both the propagation and attenuation constants. The capabilities of the method are outlined in section 3, in which some important results of the existing literature are reproduced and completed. Finally, section 4 provides several examples illustrating the potential of our approach for the engineering of practical geometries and SPP transmission line applications.

2. Numerical method

The structures considered in this study are infinitely long Ag and Au strips embedded in a lossless dielectric matrix. Their properties are investigated by numerically solving a suitably defined eigenvalue problem with HFSS (Ansoft), a 3-D finite-element commercial code. The computational domain is a box enclosing a lateral section of the waveguide, as shown in Fig. 1 in the particular case of perfectly smooth metal strips. All of the simulations presented here focus either on straight or circularly bent waveguides; the exact profile of the strip (e.g. rectangular, rounded, with or without surface corrugations) will be specified in each case.

2.1. Infinitely long and straight waveguides

We simulate an infinite structure by applying periodic boundary conditions in the direction parallel to propagation, whereas the remaining boundaries are combinations of perfect electric and magnetic walls placed far enough from the strip to leave the SPP modes unperturbed. The periodic boundary conditions ensure that the electromagnetic field on one surface of the

#9991 - $15.00 USD Received 16 December 2005; revised 31 January 2006; accepted 1 February 2006

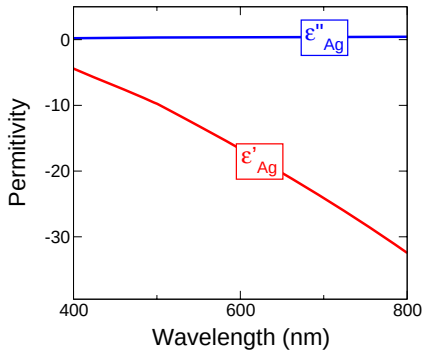

Fig. 2. Real and imaginary parts of the Ag dielectric function $\varepsilon_{Ag} = \varepsilon'_{Ag} + i\varepsilon''_{Ag}$.

computational domain matches the field on the opposite face to within a phase delay φ. A field component therefore satisfies $f(z+d) = exp(i\varphi)f(z)$, where z is the space coordinate parallel to the propagation direction and d is the distance between the two planes of periodicity. Once φ is fixed, then an eigenvalue problem is specified by the materials within the unit cell and the boundary conditions. At every value of φ, an infinite number of eigenmodes can, in principle, be obtained, each with a different complex frequency.

A serious numerical problem that occurs in the simulation of plasmonic structures is that the mode density can often become very large, with modes spaced closely in frequency. We do not present a specific solution to this difficulty here, other than to note that we make use of symmetry (both translational and reflection) to reduce the size of the computational domain as much as possible, thereby decreasing the mode density. Even our restricted computational domain can support a wide variety of cavity modes in addition to the SPP modes of interest supported by the waveguide. Therefore a careful review of the field distributions is generally required in order to identify the solutions of interest, i.e. the modes having their field localized to the metallic strip.

For the eigensolver method presented here, further numerical complications arise related to the definition of the material parameters within the unit cell. In the following simulations, we assume a lossless dielectric host with constant permittivity ε_d and a lossy metal strip with a complex dielectric function as determined from a fit to the experimental data of Johnson and Christy [24]. Figure 2 displays the fitted values of ε_{Ag}, the dielectric function of silver, as a function of the wavelength. It can be seen that ε_{Ag} is far from being constant in the visible spectrum. Once a specific value ε_{val} is assigned to a Ag strip, the computed frequency ν_0 of the mode must be consistent with $\varepsilon_{Ag}(\nu_0) = \varepsilon_{val}$ in order to be a valid solution. For each mode, we therefore adjust the initial phase delay φ between the two planes of periodicity so as to satisfy the previous equality. This self-consistency is accomplished by making an initial guess for φ and then iterating the solution. After having determined φ, the real part of the propagation constant k_{zr} can be found from the definition $exp(i\varphi) \equiv exp(ik_{zr}d)$.

The dispersion curve of the mode $\nu(k_{zr})$ is obtained by repeating the simulations for different values of ε_{Ag}; then k_{zi}, the imaginary part of the propagation constant parallel to the surface, can be calculated at any frequency according to the relation $k_{zi} \equiv 2\pi\nu"/v_g$, where $\nu"$ is the imaginary part of the frequency and v_g is the group velocity i.e. the derivative of $\nu(k_{zr})$. It should be noted that the use of periodic boundary conditions always folds the dispersion of the SPP modes when k_{zr} reaches the edge of the Brillouin zone π/d. For non-periodic systems, we work with a sufficiently small value of d (typically between 10 nm and 100 nm) so that the zone-folding occurs at frequencies beyond the spectral range we consider. It is usually

#9991 - $15.00 USD Received 16 December 2005; revised 31 January 2006; accepted 1 February 2006

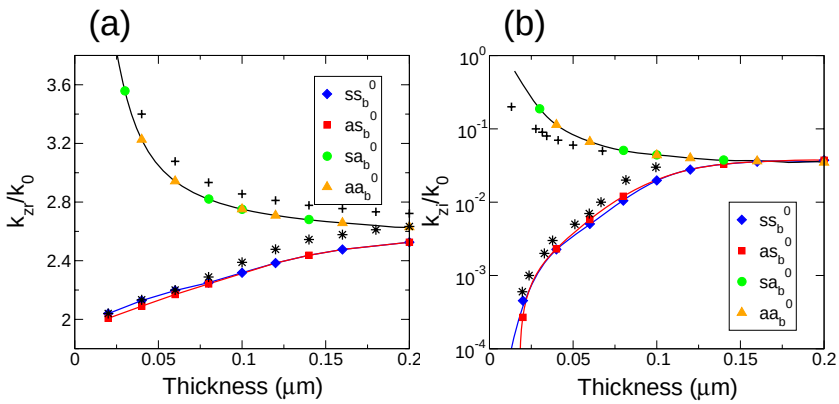

Fig. 3. Dispersion with thickness of the 4 fundamental modes supported by a straight Ag strip with rounded corners ($w = 1$ μm, $r = 5$ nm, $\varepsilon_d = 4$) at the free-space wavelength $\lambda_{vac} = 633$ nm. For comparison, we include data points from Ref. [5] for the ss_b^0 mode (black stars) and the sa_b^0 mode (black crosses) supported by a rectangular Ag strip with 90 degree corners ($w = 1$ μm, $r = 0$ nm, $\varepsilon_d = 4$).

desirable to minimize d since it reduces the size of the computational domain and thereby improves the calculation process. However, d should be non-zero even for truly 2-D problems (such as solving for the modes of the smooth rectangular waveguide of Fig. 1(a)) because we use an eigensolver for 3-D geometries.

2.2. Bent waveguides

Although our simulation method is largely independent of the waveguide geometry, the numerical analysis of bent metal strips imposes certain changes on the computational domain. An illustration of the unit cell, which consists in an arc of waveguide, can be seen in Fig. 1(b). The curved transmission line is described in cylindrical coordinates by the parameters ρ_0, the mean radius of curvature (defined as the distance between the origin of the cylindrical coordinates and the middle of the strip), and ρ_s the position of the outer surface of the unit cell; we maintain the previous notations for the width and thickness of the strip. The periodic boundary conditions applied at the edges of the unit cell are now that a field component satisfies $f(\theta_0+\theta_1) = exp(i\varphi) f(\theta_0)$, where θ_0 and $(\theta_0+\theta_1)$ are the position of the two planes of periodicity in cylindrical coordinates, and φ is the phase delay (see Fig. 1(b)). Note that when $\rho_0 \gg w$ and $\theta_1 \ll 1$, the previous equality can be approximated by $f(\theta_0+\theta_1) \simeq exp(i\theta_1\rho_0 k_{zr}) f(\theta_0)$, which provides a qualitative relationship between φ and the in-plane component of the SPP wave vector k_{zr}.

SPP transmission lines having a radius of curvature lose power by radiation. In analogy with bent dielectric waveguides [25], the electromagnetic flux arising from radiative losses is expected to cross the sole surface $\rho = \rho_s$. We accordingly surround this surface with a Perfect Matching Layer (PML)–a fictitious anisotropic material that fully absorbs the electromagnetic fields impinging upon it. PMLs essentially push the boundary infinitely far away from the structure [26, 27], thus preventing the light from being numerically reflected at the edge of the computational domain.

#9991 - $15.00 USD Received 16 December 2005; revised 31 January 2006; accepted 1 February 2006

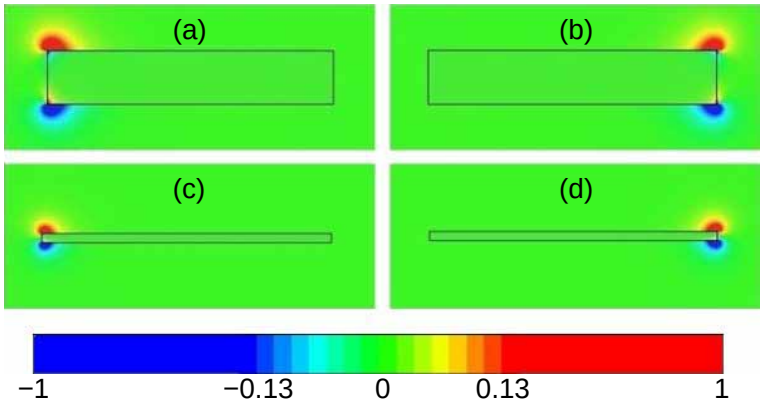

Fig. 4. Cross-section of the E_y field component for (a) the sa_b^0 mode when $t = 200$ nm; (b) the aa_b^0 mode when $t = 200$ nm; (c) the sa_b^0 mode when $t = 40$ nm; (d) the aa_b^0 mode when $t = 40$ nm. The calculations have been made at the free-space wavelength $\lambda_{vac} = 633$ nm. Note that the color scale has intentionally been saturated to reveal the field pattern.

3. Testing the simulation method

The aim of this section is to reproduce some of the key results reported by Berini in reference [5] for Ag strips having a rectangular cross-section and surrounded by a homogeneous medium of permittivity $\varepsilon_d = 4$. In this case, the field distribution of the modes must be either symmetric or antisymmetric with respect to the two symmetry planes perpendicular to the propagation direction (here we refer to the symmetry of the electric field component parallel to the *y*-direction, see Fig. 1(a)). For each of the four different field symmetries that are thus possible, a series of a fundamental and several higher-order modes can be excited along the strip in much the same way as electromagnetic modes supported by hollow waveguides. Following these considerations, each family can be generated separately by placing the proper combination of electric and/or magnetic walls halfway through the structure. Consequently only one quarter of the structure needs to be simulated, which significantly reduces the calculation time. For the eigensolver method used here–as with nearly all finite-difference or finite-element methods–the simulation of a rectangular strip is not straightforward because the sharp 90 degree corners of the structure generate strong field singularities that cannot be solved properly without using an extremely fine mesh with a large number of elements. In the following, we avoid this problem and shorten the calculation time by slightly rounding the corners of the strips. As we will see, this modification does not alter the results significantly.

Figure 3 shows the real and imaginary parts of the wave vector as a function of the strip thickness for the four fundamental modes of the structure. The modes are computed at the free-space wavelength $\lambda_{vac} = 633$ nm for strips of width $w = 1$ μm; the radius of the rounded corners is $r = 5$ nm. We have labeled the modes according to the nomenclature proposed by Berini [5] in which a pair of letters indicates whether E_y, the transverse electric field component of highest amplitude, is symmetric or antisymmetric with respect to the horizontal and vertical plane of symmetry, respectively. The subscript *b* means that the modes are bounded to the surface and the superscript indicates the number of maxima in the spatial distribution of E_y along the largest dimension.

The modes of the strip exhibit two opposite behaviors depending on whether their field component E_y is antisymmetric or symmetric with respect to the horizontal symmetry plane of the structure. In the antisymmetric case, the modes follow the upper curves of Figs 3(a)– 3(b) and

#9991 - $15.00 USD Received 16 December 2005; revised 31 January 2006; accepted 1 February 2006

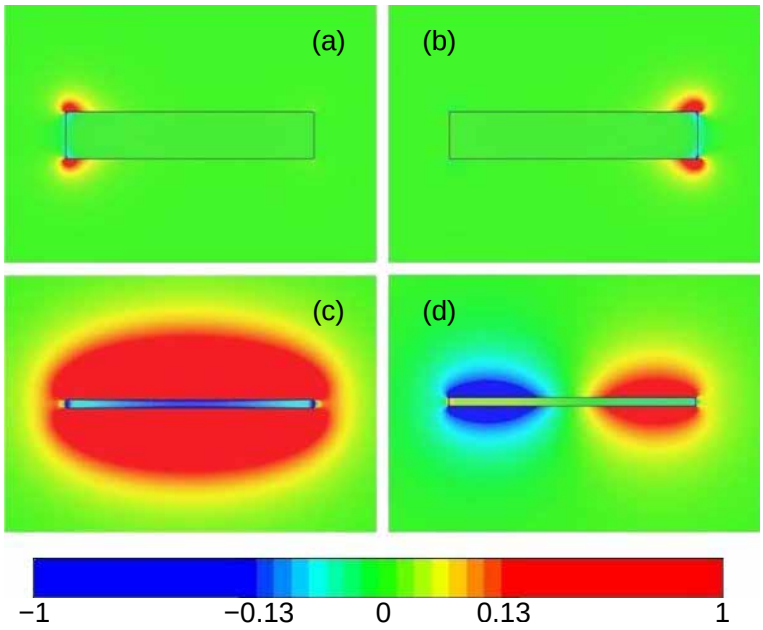

Fig. 5. Cross-section of the E_y field component for (a) the ss_b^0 mode when $t = 200$ nm; (b) the as_b^0 mode when $t = 200$ nm; (c) the ss_b^0 mode when $t = 40$ nm; (d) the as_b^0 mode when $t = 40$ nm. The calculations have been made at the free-space wavelength $\lambda_{vac} = 633$ nm.

remain degenerate for all studied thicknesses. In the symmetric case, the modes are characterized by the lower branches which eventually split as the strip gets thinner. The evolution of each branch is correlated with the field distributions of the modes. For example it has been shown that the fields of the upper branch modes remain localized near the corners and penetrate deeper into the strip with decreasing strip thickness [5]. This improving confinement results in smaller group velocities and higher damping by absorption in the metal, which in turn increases both the real and imaginary parts of the wave vector. Conversely, the fields of the lower branch modes spread around the whole structure and extend farther into the dielectric region as the strip becomes thinner. The imaginary part of the wave vector for these weakly bound, nearly TEM-like modes vanishes while the real part tends to the value of a plane wave in the dielectric material–a behavior that corresponds to the expected signature of long-ranging SPPs. It should be noted that a compromise between propagation length and field confinement will typically be required for practical applications, as one is always achieved at the expense of the other.

Maps of the electric field component E_y corresponding to the four fundamental modes are shown in Figs. 4 and 5 for the thicknesses $t = 200$ nm and $t = 40$ nm. In order to test the accuracy of our simulation technique, we solved the fields for the whole structure, without the use of perfect electric or magnetic walls along the symmetry planes of the strip. Although the different field distributions are fully consistent with the above discussion, the eigensolver finds that some modes are truly degenerate which is in contradiction to the conclusions of Berini who found all modes to be nondegenerate [5]. We see from Fig. 4 that the the upper branch modes are essentially indistinguishable, having identical frequencies and having the same field patterns, albeit localized on opposite sides of the structure. Our simulations thus indicate that the sa_b^0 and aa_b^0 modes occur as degenerate antisymmetric solutions with respect to the horizontal symmetry plane, resulting from the interaction between SPPs supported by two corners. The case of the lower branch modes supported by thick strips is similar, as illustrated in Figs 5(a) and 5(b)

#9991 - $15.00 USD Received 16 December 2005; revised 31 January 2006; accepted 1 February 2006

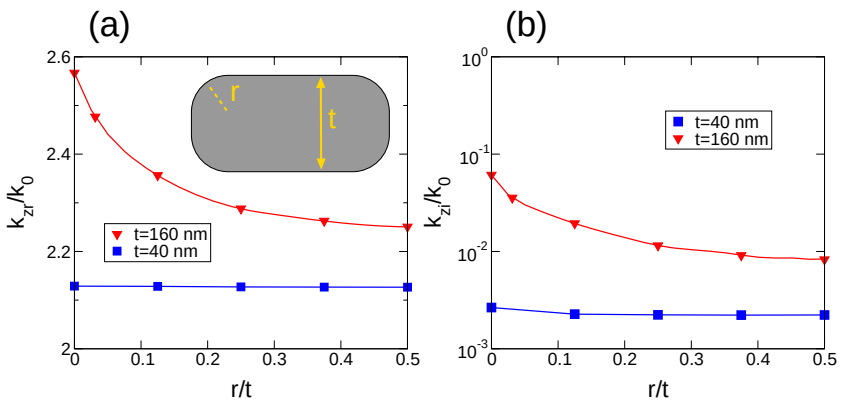

Fig. 6. Effects of rounding the corners on the ss_b^0 mode for two Ag strips with different thicknesses t ($w = 1$ μm, $\lambda_{vac} = 633$ nm). Insert: geometry of the strip.

for $t = 200$ nm. However, they represent in this case the symmetric solution with respect to the horizontal symmetry axis. In addition, the degeneracy is lifted as the thickness of the strip decreases. This is due to the fact that the fields now surround the whole structure, thus allowing the left and right side of the structure to couple.

These results are somewhat surprising when compared with Ref. [5], in which simulations for the same structure indicate that the left and right corners "remain weakly coupled" for all thicknesses, thus implying that the fundamental modes are in fact never truly degenerate for this particular strip width. Since the dispersion relations of Fig. 3 are in good agreement with Berini's, our numerical results suggest that the coupling between the left and right side of the structure becomes so weak that it cannot be resolved by the eigensolver with a manageable number of mesh points. It should be noted that such common numerical difficulties only arise when the modes are almost degenerate and can be overcome by taking advantage of the geometrical symmetry in order to minimize the size of the computational domain as outlined earlier.

We also verified that rounding the corners does not favor mode degeneracy by carefully analyzing the influence of the corner curvature on the fundamental modes. In Fig. 6 we plot the wave vector of the ss_b^0 mode as a function of the curvature for a 40 nm- and 160 nm-thick strip, respectively. Not surprisingly, for the thinnest structure, the wave vector remains almost constant (and also almost indistinguishable from the data points of Ref. [5], see Fig. 3) because the field surrounds the whole strip and therefore the general shape of the waveguide has more influence on the SPPs than its local details (see Fig. 5(c) and 5(d)). In contrast the mode supported by the thickest strip appears very sensitive to the corner geometry since both the real and imaginary parts of its wave vector decrease with rounding. This trend is correlated with a change in the mode field distribution, as mapped in Figs. 7(a) and 7(c) for the cases of 90 degree corners and for entirely rounded corners. The latter mode is not confined near the corners anymore but rather stretches along the long edge of the structure, extending deeper into the dielectric region and thus diminishing the damping by absorption in the metal. Also, the lower field confinement makes the left and right side of the structure interact significantly and thus lift the quasi-degeneracy of the modes. Interestingly, these results imply that the propagation length can be increased by rounding the corners of thick strips.

Similar remarks apply for the other modes. However, the field distribution of the fundamental short-range modes (i.e. the upper branch modes of Fig. 3) stretches along the smaller rather than the longer edge of the strip when the curvature of the corner increases (see Figs. 7(b) and 7(d)). As a result, the quasi-degeneracy of the modes is not modified. In order to explain

#9991 - $15.00 USD Received 16 December 2005; revised 31 January 2006; accepted 1 February 2006

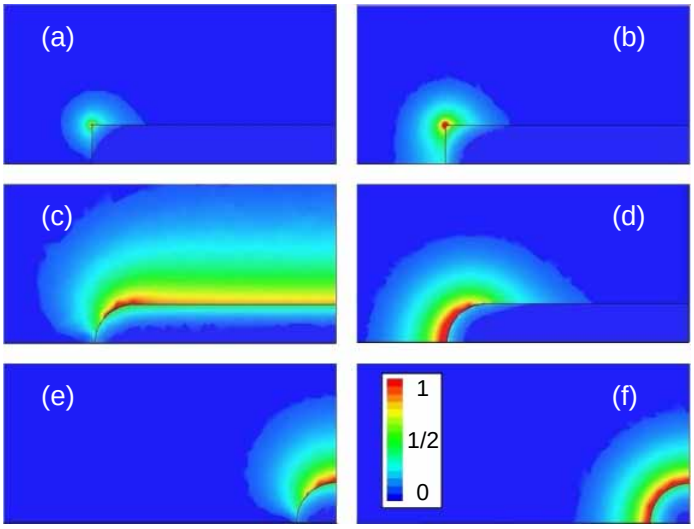

Fig. 7. Electric field distribution of the ss_b^0 mode (left panels) and the sa_b^0 mode (right panels) supported by: (a) and (b) a rectangular strip with $t = 160$ nm and $r = 0$ nm; (c) and (d) a rounded strip with $t = 160$ nm and $r = 80$ nm; (e) and (f) a cylindrical wire with $r = 80$ nm. The modes have been computed at $\lambda_{vac} = 633$ nm and the color scale is the same for all plots.

this difference, we compared these data with simulations of a cylindrical wire having the same radius of curvature (note that this problem can be solved analytically [28]). Figures 7(e) and 7(f) display the electric field of the modes exhibiting the same field symmetry as the ss_b^0 and sa_b^0 modes of the strip, respectively. For both symmetries, the field patterns surrounding the wire and the corner of the strip bear strong similarities. Hence, rounding the corners of a strip of rectangular cross-section changes the nature of the SPPs as the latter tend to the modes of a cylindrical wire having the same field symmetries. Again, this conclusion is only valid if the modes of the strip are localized near the edges. For thin strips, the lower-branch modes of Fig. 3 are long-ranging and are rather insensitive to the shape of the corner.

4. Further results and discussion

We now focus on long-range SPPs and especially on the ss_b^0 mode for the latter has been so far the only low-loss mode ever observed along a real metal strip. In the remainder of this paper, we examine some of the basic aspects of SPP transmission line engineering, namely the aforementioned problem of field confinement, the question of bent waveguides and finally the issue of surface roughness.

We will only briefly mention the question of mode confinement because solutions have already been proposed for the simplest geometries by means of semi-analytical calculations [6]. As pointed out earlier, the electromagnetic field of long-range SPP modes expands far in the dielectric matrix hence limiting in practice the degree of miniaturization of waveguide based devices. For symmetric waveguides, we have seen that any attempt to improve the field confinement (e.g. by increasing the lateral dimensions of the strip or by using a dielectric medium with a higher index of refraction) inevitably results in a dramatic increase of the losses by absorption in the metal. However the situation is somewhat different for asymmetric waveguides such as metal strips deposited on a dielectric substrate and covered by another transparent and homogeneous cladding. Long-range SPP modes are also supported in this case and typically

#9991 - $15.00 USD Received 16 December 2005; revised 31 January 2006; accepted 1 February 2006

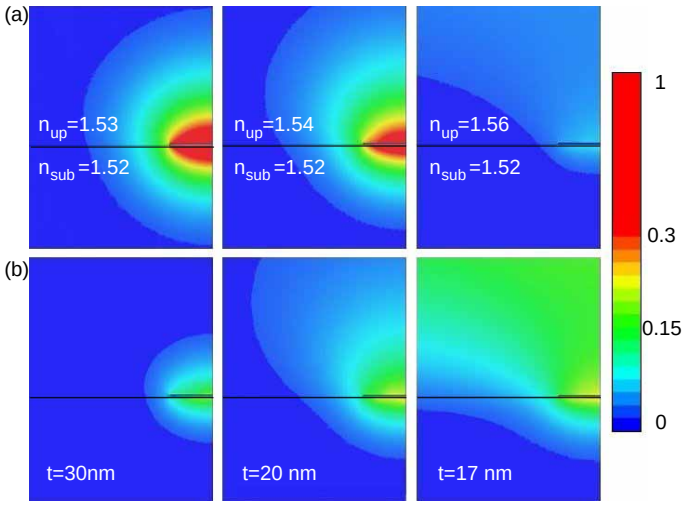

Fig. 8. Electric field distribution for Au strips ($\varepsilon_{Au} = -11.8 + i1.23$ at $\lambda_{vac} = 633$ nm) on a glass substrate. The refractive indexes of the substrate and the upper cladding are $n_{sub} = 1.52$ and n_{up}, respectively. (a) Modes supported by a rectangular strip ($w = 1$ μm, $t = 20$ nm) for increasing values of n_{up}; (b) Modes supported by rectangular strips of different thicknesses when $n_{sub} = 1.52$ and $n_{up} = 1.55$. The size of the computational domain is three to six times larger than the size of the panels.

exhibit an asymmetric field pattern due to the refractive index mismatch between the dielectric materials. This asymmetry can be exploited to at least improve the mode confinement at one side of the structure. The idea is to adjust the mismatch between the two dielectrics so that a confined mode at one interface interacts with an almost unbounded mode at the other interface– a situation that cannot be obtained in a symmetric configuration where both interfaces, and thus the modes they support, are identical. Since the resulting mode is confined at one side of the structure only, the field is not constrained into the lossy metal strip and long-range propagation can be achieved. As an example, Fig. 8(a) shows the field distribution of the SPP modes supported by a rectangular gold strip ($w = 1$ μm, $t = 20$ nm, $\lambda_{vac} = 633$ nm) for gradually higher asymmetric environments. It can be seen that the mode becomes strongly asymmetric when increasing the mismatch between the refractive indexes of the substrate ($n_{sub} = 1.52$) and the upper cladding (n_{up}). The electromagnetic field dramatically expands into the upper cladding so that the absorption losses into the metal are minimized–the propagation length increasing from 65 microns when $n_{up} = 1.53$ to 0.9 mm when $n_{up} = 1.56$. And yet, the optical field remains firmly bounded to the interface between the strip and the dielectric substrate; in fact it becomes even better confined as the asymmetry increases.

It should be noted, however, that there are definite drawbacks to working with long-range asymmetric modes. As already suggested in Ref. [6], it is probably difficult to launch these modes experimentally, for example by means of the end-fire techniques that are typically used in the case of symmetric SPP transmission lines. The end-fire coupling relies on a good field overlap between a Gaussian input beam and the SPP; this condition cannot be fulfilled by modes characterized by extended fields on one side of the strip only. Secondly, the bottom and upper interface modes that form the long-range mode have a different dispersion relation. Then the smallest variation in the material properties (see Fig. 8(a)) or in the strip shape (see Fig. 8(b)) creates a momentum mismatch between the two interface modes, which dramatically changes or even suppresses the formation of the long-range SPP. Besides the technical difficul-

#9991 - $15.00 USD Received 16 December 2005; revised 31 January 2006; accepted 1 February 2006

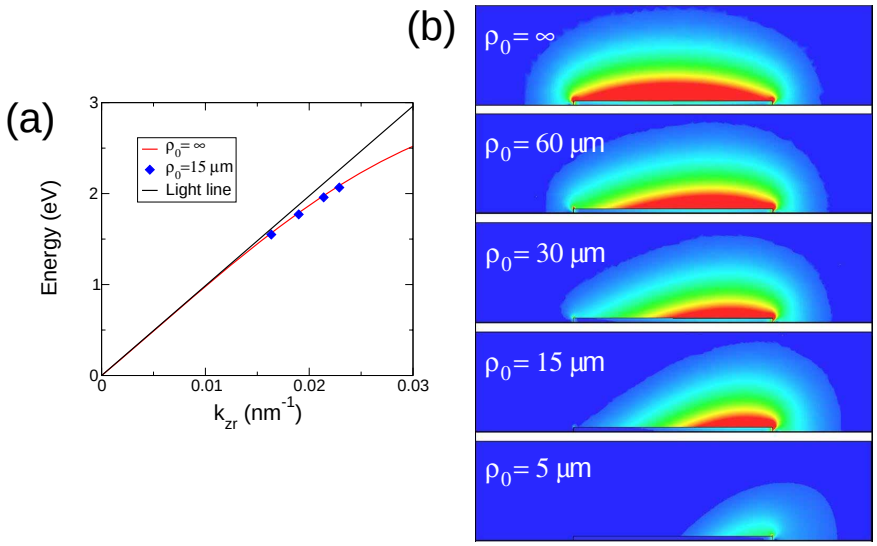

Fig. 9. (a) Dispersion with frequency of the ss_b^0 mode for a straight and a bent SPP transmission line; (b) Electric field distribution of the ss_b^0 mode for different radii of curvature ρ_0.

ties involved in operating a mode of such a high sensitivity, an obvious limitation of long-range asymmetric modes is their poor ability to support a change in the strip curvature. It is thus unlikely that a complex plasmonic circuitry might be based on an asymmetric environment.

In contrast, the ss_b^0 mode supported by symmetric SPP transmission lines can be particularly robust with regard to bending. We illustrate this point by examining the ss_b^0 mode of symmetric Ag strips ($t = 40$ nm, $w = 1$ μm, $\varepsilon_d = 4$) with various radii of curvature ρ_0. As shown in Fig. 9(a) for $\rho_0 = 15$ μm and $\rho_0 = \infty$, the mode dispersion relation remains largely independent of the radius of curvature even for very sharp bends. To gain further insight into this behavior, we map the electric field of the mode for different values of ρ_0. Figure 9(b) summarizes these simulations performed at the free-space wavelength $\lambda_{vac} = 633$ nm. As ρ_0 decreases, the field evolves from a symmetric pattern surrounding the strip to a localized and highly asymmetric distribution around the outer corner. In other words, the bending improves the field confinement and hence allows the mode to propagate without suffering significant curvature losses. It is however likely that experimental transmission lines operating in similar conditions would lose more power than what the present results suggest. Real bends are often composed of combinations of straight and curved segments, in which case transition losses between the connecting segments can become important, as suggested by the significant mismatch between the field patterns of Fig. 9(b). It would be thus interesting to analyze in detail the coupling between structures of different curvatures. This would require simulating the junction and a significant length of strip, since the geometry of the problem does not allow the efficient use of periodic boundary conditions. Unfortunately the size of the computational domain required would be too large to perform tractable simulations using the eigensolver as outlined. We note that the metal thickness and consequently the field confinement of the structures considered in this section are too large for the ss_b^0 modes to be truly long-ranging. Experimental investigations [8] at telecom wavelengths have demonstrated that curvature losses compromise the propagation of long-range modes when the radius of curvature is smaller than a few millimeters.

The performances of SPP transmission lines are also affected by the unavoidable surface

#9991 - $15.00 USD Received 16 December 2005; revised 31 January 2006; accepted 1 February 2006

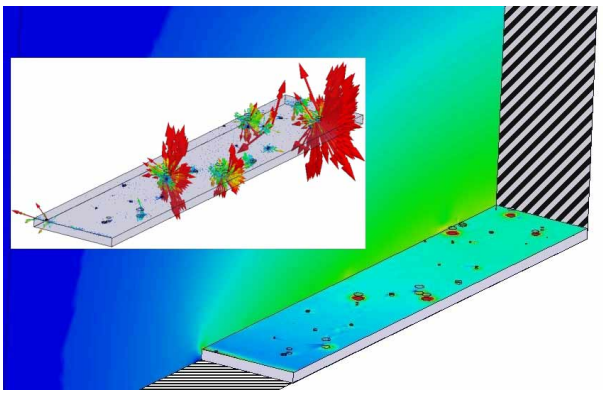

Fig. 10. Electric field pattern of the ss_b^0 mode in a plane perpendicular to propagation and in the upper plane of the Ag strip. The dashed zones are the horizontal electric wall and the vertical magnetic wall placed at the boundaries of the computational domain. Insert: Poynting vector above the surface.

roughness of real structures. A quantitative modeling of this effect is beyond the scope of this paper; however we show that some insight into the effect of surface disorder can be gained by the eigensolver techniques presented here. We consider a straight, 20 nm-thick Ag strip of rectangular cross-section surrounded by an isotropic medium ($\varepsilon_d = 4$) with a fictitious surface roughness modeled by the addition of subwavelength Ag cylinders of various sizes on the surface of the strip. The height of the cylinders is treated as a random variable with values uniformly distributed between 0 and 5 nm; in addition, the radius of the cylinders is always smaller than half their diameter. The cylinders are themselves distributed randomly; however, since the unit cell is reduced to a quarter of the actual structure with periodic boundary conditions applied in the direction of propagation, the surface roughness actually follows a periodic pattern. This approximation to the transmission line with roughened surface is compatible with our computational resources. It should be noted that a full quantitative study of surface roughness should be possible but would require the four faces of the strip to be included within the computational domain, and the distance between the two planes of periodicity larger than the scattering length of the SPP mode.

The small corrugations cause but minor perturbations to the plasmon modes, as shown in Fig. 10 for the ss_b^0 mode: the field distribution is globally similar to the case of perfectly smooth surfaces save that localized "hot spots" can be observed around the cylinders. The latter act as subwavelength scatterers, as indicated by the local Poynting vector which typically assumes all directions in the vicinity of a given perturbation. The surface roughness thus presents an additional decay channel through which the damping of the SPP is increased due to local scattering. Radiation losses, however, remain small, as can be determined by comparing the complex wave vector for the rough strip with that of the perfectly smooth strip (result not shown here; note that solutions of a given problem are multiple because the corrugations strongly increase the mode density within the unit cell so that a large number of modes, each having very similar wave vector and energy, are generated). Accordingly, the long-ranging modes are rather insensitive to small details of the strip shape which is not surprising for they are only weakly bound to the surface. This result is also consistent with theoretical data for an infinitely wide metal film [29] as well as experimental evidences that long-range modes can be excited despite the unavoidable surface roughness of real samples [7-14].

The fact that long-range modes are only little affected by a small modulation of the metal

#9991 - $15.00 USD Received 16 December 2005; revised 31 January 2006; accepted 1 February 2006

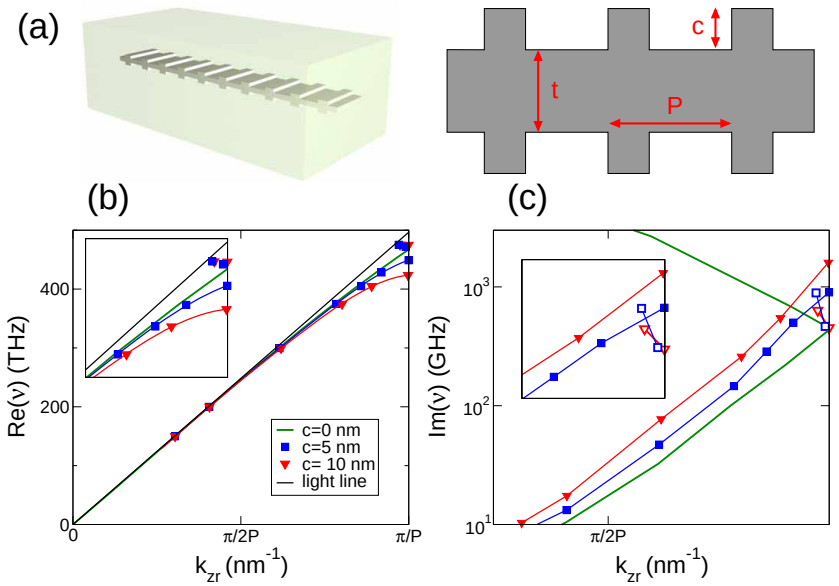

Fig. 11. (a) 3D and side views of a periodic structure with a square wave modulation ($w =$ 1 μm, t=40 nm, $P = 150$ nm). (b) Dispersion with frequency of the ss_b^0 mode for three modulation heights c. Insert: zoom of the plot near the gap region. Note that the upper bands actually cross the light line, however, the mode density within the computational domain becomes so large that the solutions of interest could not be easily identified. (c) Imaginary part of frequency vs. real part of wave-vector for the lower (plain symbols) and upper (open symbols) branches of Fig. 11(b). Insert: zoom of the plot near the gap region. The same colors have been used in all plots.

surface has to be taken into account when designing strips with specific functionalities. Typically, SPP structures can gain functionality if patterned with periodic corrugations [30, 31], which, in the context of SPP transmission lines, is of interest for filtering of signals, coupling and/or creating transmission lines with a negative effective index of refraction. In the first case, the filtering results from Bragg scattering of the SPP modes on the periodic roughness [9, 14] and from the concomitant gap opening in the mode dispersion relation. In the second case, the negative index of refraction is related to the zone-folding of certain SPP bands in the first (or higher) Brillouin zones [32, 33]. As engineered SPP transmission lines are becoming of increased interest, it is important to optimize these effects with an accurate choice of the surface modulation. We have seen that the SPP modes are only weakly scattered by very small surface corrugations, which suggests that similar periodically positioned corrugations may not be sufficient to open a bandgap in the plasmonic band structure.

To illustrate the effect of the periodicity, we study the band structure of the ss_b^0 mode supported by a periodic waveguide structure. The lattice constant P is kept constant while the effect of the modulation depth is explored. The structure consists of a Ag strip of rectangular cross-section with a square wave modulation of the top and bottom surface (Fig. 11(a)). Strictly speaking, such a surface profile contains an infinite number of spatial Fourier components which each may influence the SPP modes. However, it is known that the lowest harmonic $2\pi/P$ dominates the scattering of the SPP modes so that the role of the higher Fourier components can be ignored for sake of clarity [30]. Unlike the case of random disorder, metal strips with artificial periodic roughness are intrinsically suited for our numerical method. Given

#9991 - $15.00 USD Received 16 December 2005; revised 31 January 2006; accepted 1 February 2006

the geometry of both the waveguide and the field profile of the mode, the computational volume only includes one quarter of the strip and is otherwise filled with a lossless medium with $\varepsilon_d = 4$. The length of the unit cell in the direction of propagation is set to one period of the surface modulation. Thus, the phase advance between the two planes of periodicity is such that the corresponding propagation constant (k_{zr}) always lies within the first Brillouin zone.

Figure 11(b) shows the dispersion curve of the ss_b^0 mode for three increasing square wave modulation heights (0, 5 and 10 nm). As expected, a gap of growing magnitude opens up when k_{zr} reaches the edge of the first Brillouin zone π/P. The mode propagation at frequencies below or above the gap is significantly affected by the surface modulation depth because the scattering losses typically increase with the modulation height. Figure 11(c) illustrates this point by plotting the imaginary part of the frequency as a function of the wave vector for the different branches of Fig. 11(b).

Periodic waveguides supporting the upper branch modes could be exploited to build the optical counterparts of the left-handed transmission line metamaterials that have been demonstrated at microwave and radio frequencies [34, 35]. The property of "left-handedness," or negative refractive index, is usually associated with composite bulk materials for which the average electric permittivity and magnetic permeability are simultaneously negative [36]. The latter devices are typically arrays of LC [37, 38] or Mie [39, 40] resonators and exhibit a band pass for which the electromagnetic waves propagate as if in a medium with a negative index of refraction. In this case, the wavelengths of operation are often much larger than the periodicity so that the structure responds as a continuous material. The origin of left-handedness in periodic SPP transmission lines is somewhat different because it is a mere consequence of the Bloch theorem and doesn't involve any resonant scattering elements. It is well-known [41] that periodic structures can support Bloch waves whose group and phase velocities, $d\omega/dk$ and ω/k, respectively, have opposite sign, meaning that the energy flux points toward the opposite direction of the wave front propagation. Those waves can thus be considered as if having a negative propagation constant or as if traveling in a medium with a negative refractive index. This is exactly the case for the upper branch modes of Fig. 11(b) so they can exhibit many of the interesting and unusual properties initially proposed for bulk metamaterials.

5. Conclusion

We have presented a simulation tool for modeling SPP transmission lines. Based on solving an eigenvalue problem, this method can be used to compute the modes for a wide variety of structures, as suggested by the different examples examined in this article. This versatility is of potential interest for designing engineered SPP waveguides and new plasmonic structures.

Acknowledgments

This work was performed under a Multiple University Research Initiative supported by the Air Force Office of Scientific Research (Contract Number FA9550-04-1-0434).

#9991 - $15.00 USD Received 16 December 2005; revised 31 January 2006; accepted 1 February 2006